

Gamma (γ)-Ray Activity as a Tool for Identification of Hidden Ejecta Deposits Around Impact Crater on Basaltic Target: Example from Lonar Crater, India

T. Bose · S. Misra · S. Chakraborty · K. Reddy

Received: 12 October 2011 / Accepted: 16 August 2013 / Published online: 26 September 2013
© Springer Science+Business Media Dordrecht 2013

Abstract Geophysical techniques based on radioactivity measurements are not generally used for exploration of asteroid impact craters. Our studies on the field and laboratory measurements of radioactivity on samples from the Lonar crater, India, show that this technique could be an important method for mapping the distribution of ejecta around the deeply excavated impact craters particularly when these structures are formed on relatively old target rocks/palaeosol. The Lonar ejecta shows ~ 1.3 times higher γ -ray count rates in the field on average compared to the underlying palaeosol and ~ 1.9 times higher values over the target basalt while measured by a portable Geiger–Müller pulse counter. The absorbed γ -dose rate (D) of the Lonar samples, computed from ^{232}Th , ^{238}U , and ^{40}K abundances in these samples, also show that the ejecta has distinct bulk dose rates (average $\sim 8.42 \text{ nGy h}^{-1}$) as compared to those of the palaeosol ($\sim 18.34 \text{ nGy h}^{-1}$), target basalt ($\sim 11.97 \text{ nGy h}^{-1}$), and the impact-melts and spherules ($\sim 14 \text{ nGy h}^{-1}$). Therefore, radioactivity mapping of the terrestrial and planetary impact craters by direct methods has importance in mapping ejecta distributions around these structures.

Keywords Lonar crater · Palaeosol · Ejecta · Geiger–Müller pulse counter · Gamma-radiation · Absorbed γ -dose rate (D)

1 Introduction

The Lonar crater, India, centered at $19^{\circ}59'\text{N}$, $76^{\circ}31'\text{E}$ (Fig. 1a, b), is a relatively young asteroid impact crater that formed $570 \pm 47 \text{ ka}$ ago by an oblique impact of a chondritic

T. Bose · S. Chakraborty
Indian Institute of Tropical Meteorology, Pune 411008, India

S. Misra (✉)
School of Geological Sciences, SAEES, University of KwaZulu-Natal, Durban 4000, South Africa
e-mail: misras@ukzn.ac.za; saumitramisra@yahoo.co.in

K. Reddy
National Geophysical Research Institute, Hyderabad 500007, India

asteroid on the almost flat basaltic target rock from the east (Nayak 1972; Fredriksson et al. 1973; Misra et al. 2009, 2010; Jourdan et al. 2011). The target rock of this crater is the Deccan Trap basalt that erupted in a very short interval of time at or near the Cretaceous-Tertiary boundary at 65 ± 0.9 Ma (Hofmann et al. 2000; also see Courtillot et al. 2000; Chenet et al. 2007) or close to 67.4 ± 0.9 Ma (Pande et al. 2004). The Lonar crater is perhaps one of the few known terrestrial impact craters on a basaltic target, and therefore has importance in evaluating extra-terrestrial impact craters on planetary surfaces having basaltic crusts. The other one is the Logancha crater, Russia, which could be on the Siberian Trap basalts (Reichow et al. 2002), but little information is available on this crater (Feldman et al. 1983; Masaitis 1999). The most recently known impact structure in a basaltic target is the Vista Alegre crater on the Paraná flood basalt (approximately 133–132 Ma), Brazil (Crósta et al. 2010).

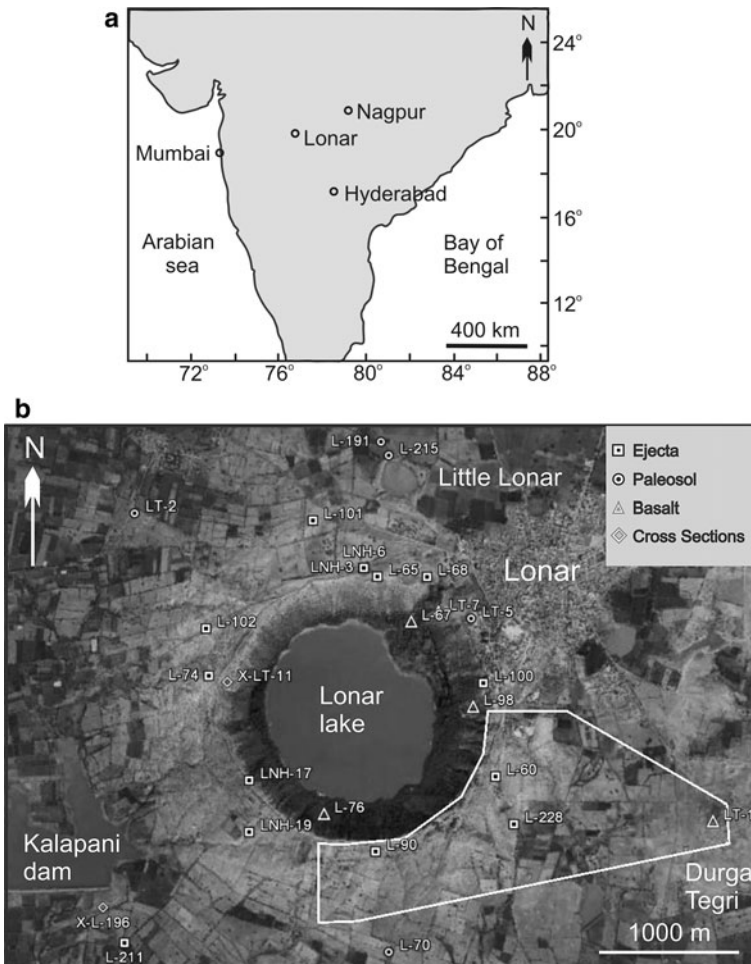


Fig. 1 a Schematic map of India showing the position of Lonar impact crater, India; b the map after Google Earth of the Lonar crater (2013) showing the sample locations for the present study, the part within the white outline is the zone of detail investigation

The Lonar crater is a bowl-shaped, simple impact crater, having E–W and N–S diameters of $\sim 1,832$ and $1,790$ m respectively, with circularity of ~ 0.95 (Fig. 1b), and a depth of ~ 150 m at present (Fredriksson et al. 1973; Fudali et al. 1980; Koeberl et al. 2004; Kumar 2005; Misra et al. 2010). All around its circumference, except for a small sector along the NE, there is a continuous raised rim that is ~ 30 m high above the adjacent plains, while the crater floor lies ~ 90 m below the pre-impact surface. The rim is surrounded in all directions by a continuous ejecta deposit that extends outward with a very gentle slope of $2\text{--}6^\circ$ to an average distance of $\sim 1,350$ m (Fudali et al. 1980). Recent observations show that the ejecta cover extends over an area of ~ 6.7 sq. km. and to ~ 700 m in all directions except to the west where it extends for over 1 km (Misra et al. 2010). The ejecta deposit consists of angular blocks of basalt of variable sizes cemented by very fine ejecta and the maximum size of the blocks is measured up to 5 m in diameter. It is suggested that this continuous ejecta blanket around the crater rim is unique in its excellent stage of preservation (Fudali et al. 1980). The core of the depression is occupied by a shallow, saline lake; a sequence of ~ 100 m unconsolidated sediments were reported below the lake water, which overlay the highly weathered trap (Nandy and Deo 1961; Fredriksson et al. 1973). About ~ 700 m north of the rim, there is another relatively small, shallow depression, known as the Little Lonar, which has a diameter of ~ 300 m, and surrounded by a raised rim only along its southern and western margins at present. Although it was suggested that the Lonar crater and Little Lonar might have been formed together by near-simultaneous double impacts of fragments of the same bolides (Master 1999), drilling into this structure and studies on the ejecta sequences around this structure revealed no evidence of impact (Fredriksson 1999, pers. comm., Maloof et al. 2010).

A better understanding of the direction and angle of asteroid impact is one of the important aspects in evaluating the formation of an impact crater. The crater morphology that can give the best evidence on the possible projectile path is the distribution of ejecta around the crater rim, which is sensitive to angle of asteroid impact (Pierazzo and Melosh 2000; Schultz et al. 2007). The other parameters that can also be used to evaluate the oblique impact are the structural deformations of the central peak (Scherler et al. 2006) or the crater rim (Misra et al. 2010). The Lonar crater has been geologically investigated by several workers (e.g., Nayak 1972; Fredriksson et al. 1973; Fudali et al. 1980; Ghosh and Bhaduri 2003; Kumar 2005; Maloof et al. 2010), however no consistent geological map on the distribution of the ejecta blanket around the crater rim is available at present. For example, the distribution maps of the ejecta around the rim of Lonar crater, either based on the geological field work (Ghosh and Bhaduri 2003; Maloof et al. 2010) or in combination with studies on satellite imageries (Misra et al. 2010), are quite different from each other. The difficulty that exists in precise mapping of the ejecta, particularly the distant ejecta, is the weathering that diminishes the visual differences between the light gray coloured ejecta from the underlying and surrounding reddish-black coloured palaeosol (Misra et al. 2010). Distant isolated ejecta bodies are very difficult to identify due to ongoing agricultural activity. The remote sensing images have also been used to map the distribution of continuous ejecta deposited around the Lonar crater rim (Misra et al. 2010), but this technique has limitations, particularly in identifying distant isolated ejecta because the top-most target-basalt and ejecta deposits have similar reflectance in these images, and the distant ejecta along the periphery of the continuous ejecta around the Lonar crater rim has tarnished into the reddish black colour due to weathering in many cases. Fudali et al. (1980) identified discontinuous patches of ejecta and large secondary craters beyond the continuous ejecta around the Lonar crater rim within a distance of ~ 3 km, however, no geological map on this ejecta distribution or secondary craters is available.

The black-coloured palaeosols around the crater that were developed by in situ weathering of the Deccan Traps during the last ~ 65 Ma are in much more advanced stages of weathering than the much younger ejecta deposits (Newsom et al. 2007, 2010). The Lunar crater is situated in a semi-arid region with low annual rainfall (600–800 mm per year; IMD 2013) and the plateau like topography inhibits water retention over land. Hence, it can be concluded that these soils, in principle, have lost most of their soluble U and K during their formation by prolonged weathering of the target basalt (cf. Faure 1986), and expected to have comparatively low radioactivity compared to that of the overlying ejecta, which was formed primarily by extreme pulverization of the target basalt due to impact where lower and relatively unweathered target materials lying below the zone of weathering were brought to the surface. With this background information, the palaeosol and continuous ejecta deposit around the crater were measured for radioactivity both in the field and in the laboratory, and the possible outcome of this study of the indirect mapping of the ejecta around the crater rims will be discussed in the present paper.

The distributions of impact-melt bombs and spherules within the ejecta around the Lunar crater are very restricted in occurrence at present (Malooof et al. 2010), and they occupy ~ 1 volume % of the total ejecta (Ghosh and Bhaduri 2003). The impact-melt bombs occur only in small areas to the southeast, north and west of the crater close to the crater's rim (Malooof et al. 2010). The scanty occurrences of small pieces of impact-melt bombs and spherules within the ejecta around the crater's rim are also reported in the literature (Koeberl et al. 2004; Son and Koeberl 2007). Therefore, further study around the Lunar crater for any fresh deposit of impactites is needed. We therefore carried out a radioactive survey on the impact-melt bomb-rich ejecta zone at the southeastern part of the crater rim (Fig. 1b) just to examine any possible characteristic radioactivity of this area. The earlier reports on radioactivity measurements on the samples of Ivory Coast tektites and their source rock samples from the Bosumtwi crater, however, are not very convincing because crater-rocks and tektites show similar abundances of U, Th and K (Rybach and Adams 1969). For Lunar impactites, a better result is expected because these impact melt bombs were suggested to have formed by feldspar-dominated partial melting of the target-basalt (Ghosh and Bhaduri 2003; Misra and Newsom 2011), which relatively enriched these melts in U, Th and K because feldspar could be a major source of these incompatible elements in basaltic rocks (White 2005, Chapter 7).

2 Methodology

2.1 Field Observations

The gamma (γ) radiation of the Lunar palaeosol and ejecta was measured in the field using a portable Geiger–Müller (G–M) pulse counting system of United Kingdom Atomic Energy Division (Type 975011-1) with G-M probe type 978005-1 (for a description of the instrument see Sengupta et al. 2005). The instrument counts the radioactivity levels (mainly γ -ray) that are recorded on the receiver (~ 1 cm² area) held ~ 2 – 3 cm off the target surface for a pre-designated time period. The time period during our measurements was decided as 1 min and all readings were normalized for this duration. Multiple readings (>4) were taken at each spot and the final reading was the average of all these values. The instrument was used before in eastern Singhbhum, India, and found to be accurate for count rates <50 counts/min (Sengupta et al. 2005). The background radioactivity and instrument noise level is confirmed by readings towards air parallel to the ground at ~ 1.5 m height as zero.

Selected samples of fresh target basalts, palaeosol, ejecta and impact-melts were collected from the field for laboratory studies. We collected the palaeosol and ejecta samples mostly from the anthropogenically uncontaminated and undisturbed areas, and we avoided or removed the weathered part of the samples, if any, for our study.

2.2 Analytical Techniques

The laboratory measurements of radioactivity of the Lonar samples (Table 1) were done at the National Geophysical Research Institute, Hyderabad, India, by one of us (K. R.). The basic sensor was a NaI (Tl) crystal with a diameter of 5 inches and height 6 inches. It was hermetically sealed and coupled to a photomultiplier tube of 5 inches diameter. The two, along with a dynode chain and a pre-amplifier constituted the detector assembly. This was housed in a lead shield of 7 inches thick lead all around. The detector was placed in such a way that a sample canister could be placed centered over the flat part of the crystal while very close to the detector. The sample could be placed over the detector, every time with the same geometric configuration because it was arranged to sit tight fit in an aluminum ring. The lead shield cave had a door through which the sample was placed over the detector, and when closed the door also presents nearly seven inches of lead. The cables were fitted to the detector assembly: (1) which supplied high voltage, around 700 V, to the dynode chain, (2) which supplied required voltage (24 V DC) to the preamplifier, and (3) which collected the final signal from the detector. The output from the detector, a signal resulting from γ -ray interaction with the crystal, was connected to a personal computer for further processing of data. The resulting γ -ray spectrum in terms of channel number versus counts was displayed on the PC monitor.

Table 1 Concentrations of natural radioactive elements and calculated dose rates (D) for samples measured during this work

		Th (ppm)	U (ppm)	K (wt%)	D (nGy/h)
Basalt	L-76	1.80	1.80	0.30	17.95
Basalt	L-73	1.50	0.80	0.30	11.48
Basalt	L-98	2.70	1.60	0.30	19.06
Basalt	L-67	1.70	0.50	0.30	10.27
Basalt	LT-1	1.32	0.72	0.14	8.89
Basalt	LT-72	1.84	0.97	0.30	13.31
Palaeosol	L191	5.17	0.79	0.73	25.17
Palaeosol	L196PM	2.99	0.70	0.13	12.91
Palaeosol	L62	1.41	0.21	0.56	10.59
Palaeosol	L-196 P/M	3.70	1.20	0.20	18.24
Palaeosol	L-196 P/T	3.00	1.30	0.20	14.93
Palaeosol	L-215	5.10	1.80	0.90	23.07
Palaeosol	L-70	3.10	0.80	0.30	12.35
Palaeosol	LT-2	3.67	1.09	0.16	15.43
Palaeosol	LT-5	8.51	1.92	1.04	32.35
Ejecta	L-228E	2.20	0.30	0.30	7.25
Ejecta	L-211 E	1.50	1.10	0.30	10.02
Ejecta	L-102 E	2.20	0.90	0.30	10.65

Table 1 continued

		Th (ppm)	U (ppm)	K (wt%)	D (nGy/h)
Ejecta	L-196 E	1.50	1.80	0.20	13.98
Ejecta	L-60 EP	2.10	0.90	0.40	10.40
Ejecta	LT-11	2.80	0.46	0.11	9.67
Ejecta	LT-12	0.87	0.53	0.03	5.20
Ejecta	L60	2.39	0.42	0.36	8.42
Ejecta	L101	2.00	0.50	0.27	7.87
Ejecta	L74	1.52	0.32	0.42	5.65
Ejecta	L90	2.53	0.38	0.22	8.52
Ejecta	L100	2.31	0.40	0.12	8.11
Ejecta	L196E	1.93	0.46	0.22	7.46
Ejecta	L65	1.72	0.36	0.32	6.37
Ejecta	L68	1.66	0.35	0.27	6.16
Ejecta	LNH17	2.45	0.36	0.24	8.25
Ejecta	LNH19	2.40	0.50	0.12	8.90
Ejecta	LNH3	2.34	0.47	0.17	8.58
Ejecta	LNH6	2.34	0.47	0.28	8.53

Sample numbers L-60 to LNH6 and L191, L196PM, L62 are personal samples of S. Misra and H. Newsom, which were analysed by XRF (K_2O wt%) and ICP-MS (Th, U in ppm) techniques. Rest were measured using gamma spectroscopic method by K Reddy in NGRI

With the above laboratory set up, samples with the composition of Th down to ~ 1 ppm and U down to 0.5 ppm, and also granitic rocks with very high levels of Th, U and K up to 0.1 wt% could be analyzed. For Th, U and K analysis, three energy windows were chosen corresponding to the 0.911, 0.964, and 0.969 MeV peaks due to ^{228}Ac , a daughter of the ^{232}Th series; the 1.76 MeV-peak due to ^{214}Bi , a daughter of the ^{238}U series, and 1.46 MeV-peaks due to ^{40}K . The widths of the windows were chosen to minimize the interference from other nuclides. The count rates (counts/minute) were obtained by counting in the above three windows for standards, namely U, Th and K and the unknown sample.

In spite of the lead shield, there was a persistent background radiation after attenuation through the lead due to cosmic radiation, atmospheric radiation, potassium present in the crystal and also the components of the detector materials. The background counts were not from the sample. The background count rates were also obtained under the same windows by keeping the sample chamber empty for several hours. The errors in the counts with the standards were made negligibly small with sufficiently long counting times over hours. The counts from the unknown samples were also measured under similar conditions for sufficiently long time to minimize the error. The background count rates were deducted from the count rates obtained under the corresponding windows of the standards and the unknown sample. The Th, U and K concentrations in the unknown sample were computed from the peak count rates of Th, U and K of the sample and the standard (obtained from the U. S. Atomic Energy Commission) at 1.46, 1.76 and 2.62 MeV by using the equation shown in Rao (1974).

The absorbed Dose rate (D) of each sample was computed from its measured Th (ppm), U (ppm) and K (wt%) data using the standard formula after UNSCEAR (1993, 2000) (Eq. 1).

$$D(\text{nGy/h}) = 0.621 \times c_{\text{Th}} + 0.462 \times c_{\text{U}} + 0.0417 \times c_{\text{K}} \quad (1)$$

where, D = absorbed γ -dose rate in nano Gray per hour (nGy h^{-1}), and c_{Th} , c_{U} and c_{K} are activity concentrations of ^{232}Th , ^{238}U and ^{40}K in Bq kg^{-1} respectively.

The activity concentrations could be calculated from the chemical abundances of Th (ppm), U (ppm) and K (wt%) using the following relations: 1 ppm Th corresponds to 4.04 Bq kg^{-1} of ^{232}Th , 1 ppm U corresponds to 12.36 Bq kg^{-1} of ^{238}U , and 1 wt% of K_2O corresponds to 252 Bq kg^{-1} of ^{40}K (Rao et al. 2009).

3 Field and Laboratory Data

3.1 Field Data

For our field measurements, we examined ejecta and palaeosol mostly in those cross-sections and locations that were dry and showed no effect of anthropogenic activities. At the west ($\sim 500\text{m}$) of the Lonar crater rim (Fig. 1b, location X-LT-1), the cross sectional profile of the ejecta was examined in a well section where $\sim 2.3 \text{ m}$ thick ejecta overlay on a weathered target basalt (Fig. 2a). The grayish white-colored ejecta had altered to reddish or orange-colored masses at the top due to weathering. The unaltered part of the target basalt at the base of the section, gave a γ count rate of ~ 15 counts per minute (counts/min) with a standard deviation of ± 3 . The ejecta horizon gave a still higher count rate of 26 ± 3 counts/min and the value is reduced to 16 ± 3 counts/min in the weathered ejecta zone at the top.

The best preserved cross-section of the Lonar ejecta is preserved at the southwest of the crater near the Kalapani dam (Fig. 1b) (Misra et al. 2010). A 1.47 m thick, reddish-black palaeosol overlying weathered trap basalt, was covered by a $\sim 1 \text{ m}$ thick layer of light-colored fine ejecta at the top (Fig. 2b). This ejecta layer, which contained a few centimeter-sized angular basalt pebbles, tapers away towards the west within a distance of $\sim 7\text{--}10 \text{ m}$. On the continuation of this ejecta layer there was a cover of a discontinuous layer of younger soil horizon of 0.5 m maximum thickness that had similar reflectivity to that of the ejecta and consisted of eroded ejecta components only. A couple of meters further west, where the ejecta cover had tapered away, the newly formed soil horizon directly overlay the underlying palaeosol. The γ values for the palaeosol measured in four sections have an average count rate of 21 ± 2 counts/min. The overlying ejecta, however, had relatively high γ count of 29 ± 3 counts/min. The newly formed soil cover, which consists only of the eroded ejecta, had a γ count of 19 ± 3 counts/min (Fig. 2b).

A section of $\sim 2 \text{ km}$ length and $\sim 200 \text{ m}$ width from the hillock Durga Tegri at the east of the Lonar crater to the crater rim (Fig. 1b) was selected for the surface measurements. Our investigation showed that there was a $\sim 1\frac{1}{2}$ times increase of field γ -radiation from palaeosol to ejecta (Fig. 3a). While palaeosol had showed a γ -radiation between 17 and 23 counts/min, the ejecta had count rates in the range of 25–40 counts/min, observations on the ejected basaltic blocks embedded in ejecta blanket mostly showed lower γ -ray counts ($\sim 20\text{--}25$ counts/min). This increase of radioactivity is better depicted in a plot of longitude versus γ radiation along the east–west A A' section of Fig. 3a (Fig. 3b). The figure shows there is a gradual increase of γ radiation from the basalt to the palaeosol and to the ejecta. Our observation on a bigger surface area on the ejecta at the south-eastern part of the crater rim (Fig. 1b), which also includes the above section (A A'), also produced similar type of results, i.e. increase of γ -radiation from the target basalt to the palaeosol and to the ejecta towards the crater rim (Fig. 3c). The latitude versus γ -radiation plot along the

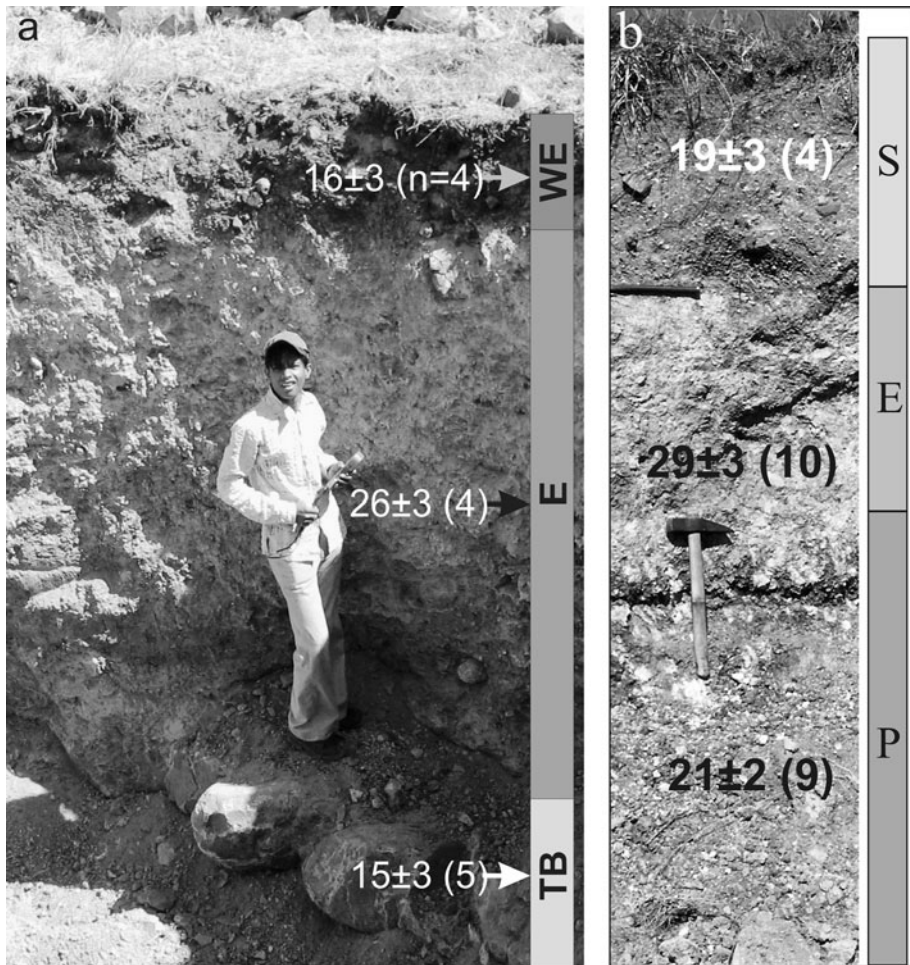


Fig. 2 **a** A freshly dug well to the west of the Lonar crater showing target basalt (*TB*) at the base, the overlying ejecta (*E*) and weathered ejecta (*WE*) at the top; **b** the soil cross-section exposed in a canal near the Kalapani Dam at the southwest of the Lonar crater showing palaeosol (*P*), ejecta (*E*) and soil derived from ejecta (*S*) in the stratigraphic younging direction; note the average γ -counts in different layers; numbers in parentheses are numbers (*n*) of respective measurements

north–south B–B' section of Fig. 3c clearly shows this variation (Fig. 3d). We also attempted to extend our observation in north of Lonar crater (Fig. 1b), but the area was heavily contaminated by farming and sewerage, and hence the data from this area were not reliable enough for any meaningful conclusion.

The ejecta blanket to the east of the Lonar crater rim (Fig. 1b, L-60) showed presence of small pockets of impact-melt bombs (Misra et al. 2009). We had altogether 10 sites of measurements on this zone. Our data suggest that the impact-melt bomb bearing ejecta in this area had nearly the similar count rates of ~ 26 – 33 counts/min in comparison to the ejecta having no known hidden impact-melt deposit. The individual impact-melt bombs within the ejecta, however, produced relatively low count rates of ~ 20 counts/min, which is, however, higher than the fresh target-basalt (~ 11 – 15 counts/min).

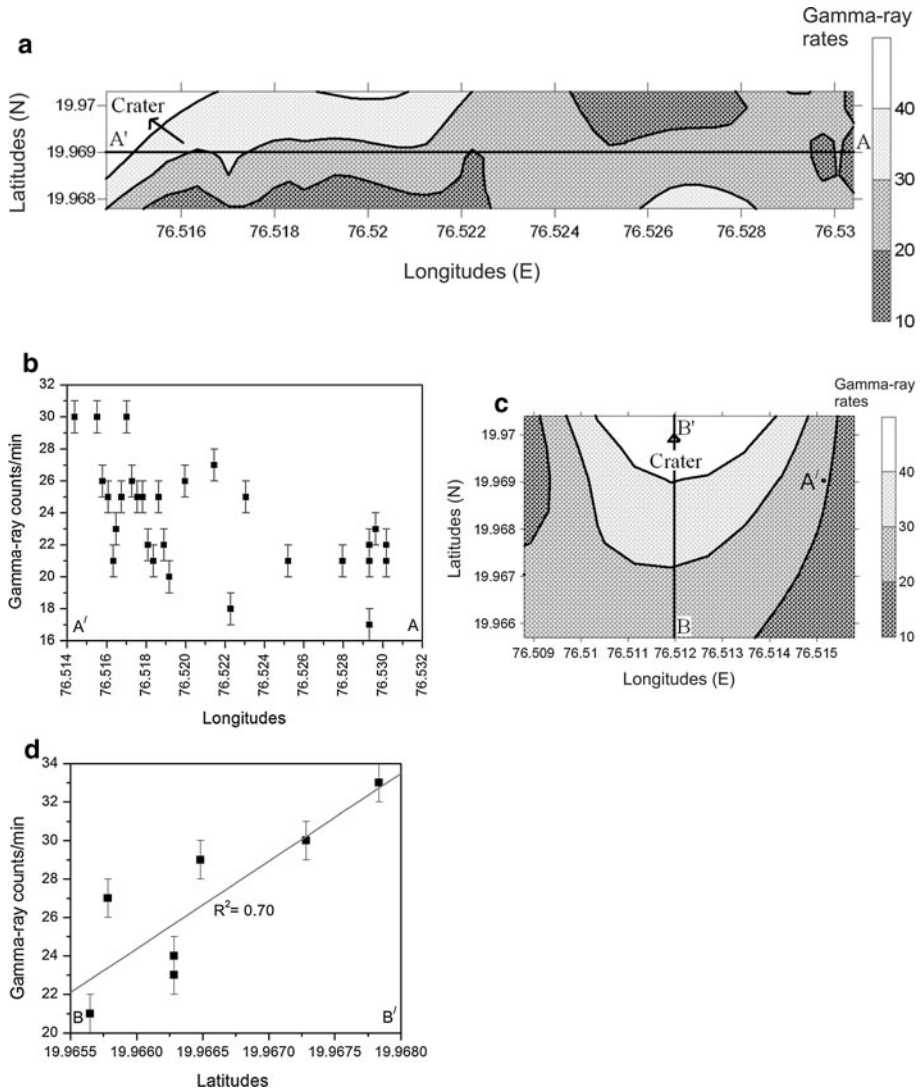


Fig. 3 **a** Contour plot of γ -activity in the SE section of the Lonar crater (number of our field measurements = 56), **b** plot of variation of γ -activity against longitudes along section A'A' of figure **a**, **c** contour plot of γ -activity in the South section of the Lonar crater (number of field measurements = 9), note the position of A' of figure **a** for reference, **d** plot of variation of γ -activity against latitudes along section BB' of Fig. 3c. The basic data for the γ -activity contour maps for figures **a** and **c** are given in "Appendix"; error associated with individual measurement is ± 1 count/min

A summary of our observation on radioactivity of the target-basalt, palaeosol, ejecta and soil derived from the ejecta is shown in Table 2 and Fig. 4. The ejecta has the highest average count rate (\pm standard deviation) of 28 ± 3 counts/min (range of data ~ 24 – 35), followed by palaeosol of 22 ± 2 counts/min (range ~ 16 – 26 counts/min), modern soil (derived from the ejecta) of 18 ± 3 counts/min (range ~ 15 – 22 counts/min) and target basalt of 15 ± 2 counts/min (range ~ 11 – 17 counts/min).

Table 2 The average values of γ -radiation observed in the field for the target basalt, palaeosol, ejecta, and modern soil above ejecta

Lithotypes	Number of locations	Number of measurements	Average \pm standard deviation
Basalt	4	12	15 \pm 2
Palaeosol	8	19	22 \pm 2
Ejecta	12	22	28 \pm 3
Modern soil above ejecta	3	4	18 \pm 3

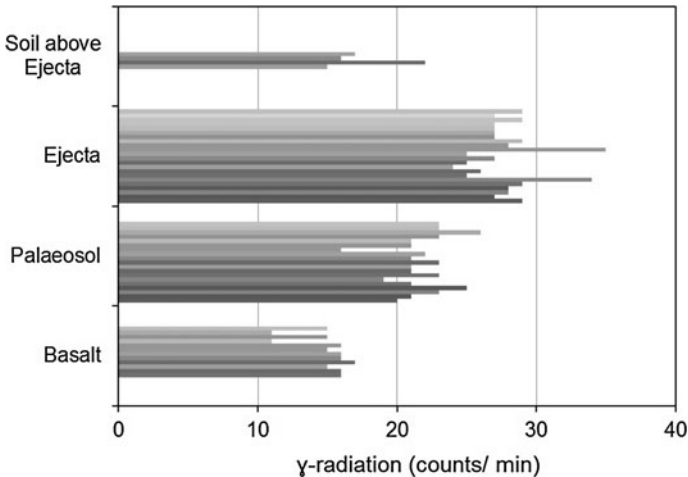


Fig. 4 Bar diagram showing variation of γ count rates for different litho-units in field around Lonar crater

3.2 Laboratory Measurement on Radioactivity

The Th (in ppm), U (ppm) and K (wt%) contents of the ejecta, palaeosol and target basalt samples from the Lonar crater (Fig. 1b) are given in Table 1, and their relative geochemical variations are shown in Fig. 5. Additional data for these plots are collected from literature (Osae et al. 2005; Son and Koeberl 2007; unpublished data of H. Newsom and S. Misra). The average Th content is the highest for the palaeosol with relatively high variation ($n = 9$, average \pm standard deviation: 4.07 ± 2.02 ppm), followed by the impact-melt ($n = 72$, 2.52 ± 0.39) and impact-spherule ($n = 7$, 2.53 ± 0.27), ejecta ($n = 19$, 2.04 ± 0.47) and target-basalt ($n = 26$, 1.89 ± 0.48). The average U content is also found to be the highest in the palaeosol (1.09 ± 0.54), the rest of the samples including impact-melt (0.65 ± 0.36), impact-spherule (0.55 ± 0.17), ejecta (0.58 ± 0.37) and target basalt (0.67 ± 0.38) have very similar averages with wide ranges of variation in the most of the cases except the impact-spherule. The average K contents of the palaeosol (0.47 ± 0.35), impact-melt (0.46 ± 0.10) and spherule (0.40 ± 0.11), are close to each other, which are followed by the target-basalt (0.32 ± 0.15) and ejecta (0.24 ± 0.10).

In the K (wt%) versus Th (ppm) plot, the target basalts define a very gentle linear increasing trend for Th with increasing K (Fig. 5a). The majority of the ejecta samples define a population on this linear array of target basalt with $K < 0.37$ wt%. The impact-melts along with impact-spherules form a different population just above the linear array

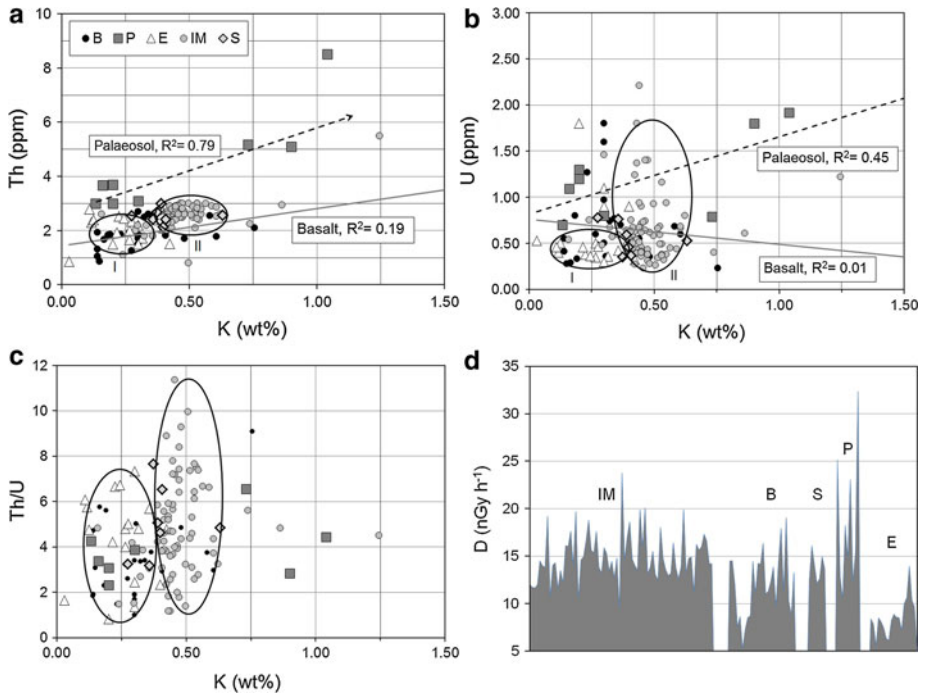


Fig. 5 Geochemical variation of samples from Lonar crater in K (wt%) versus **a** Th (ppm), **b** U (ppm), and **c** Th/U ratios; **d** bar diagram showing the variations of computed absorbed γ -dose rate (D) of Lonar samples. Abbreviations B-target basalt, P-palaeosol, E-ejecta, IM- impact melt, S- impact spherule, I and II represent fields of distribution of ejecta and impact-melt respectively in the discussed geochemical fields. Data from Osae et al. (2005, the impact-melt samples considered for this study are L-22, L-23, L-29, GSI-1, SG-1, SG-2, SG-3), Son and Koerberl (2007), unpublished data of H. Newsom and S. Misra, and data from Table 1

defined by the target-basalt with $K > 0.30$ wt% in the majority of the cases. The overlap between the fields described by the majority of ejecta and impact-melt samples is minimum and the majority of the impact-spherule samples are plotted in the interface zone between the two fields. The Th contents of palaeosol samples are always found to be higher than the other Lonar samples for any specific value of K. Our limited number of palaeosol samples describes a possible linearly increasing trend for Th with increasing K.

In the K versus U plot, the target basalts describe an ill-defined linear decreasing trend for U with increasing K (Fig. 5b). The most of the ejecta samples, having K less than 0.37 wt%, produce an elliptical cluster in this diagram where U contents of the ejecta samples are marginally lower than that on the trend described by the target basalt. The majorities of the impact-melt samples are plotted on or close to the linear trend defined by the target basalt, and form an elliptical cluster that marginally overlaps with the field described by the ejecta, with a wide variation in U from ~ 0.25 to 1.75 ppm. The majority of the impact-spherule samples are plotted on the boundary between the fields of the ejecta and impact-melt. Like Th, the palaeosol samples also show relatively high U contents over the other Lonar samples and there could be a linear increasing trend of U with increasing K for these samples.

The Th/U ratios of the target basalt samples show a wide variation between ~ 1 and 6, although this variation is higher in ejecta between ~ 1 and 7, and the highest in the impact-melt samples between ~ 1 and 11 (Fig. 5c). The geochemical fields defined by the ejecta and the impact-melt are almost non-overlapping, and the impact-spherule samples are plotted close to the boundaries of these two fields. The palaeosol samples in the majority of cases are plotted within the field of ejecta and these samples show the least variation in Th/U mostly between ~ 2 and 4. Three samples of palaeosol with $K_2O \geq 0.75$ wt%, however, show higher variation of Th/U between ~ 3 and 7.

We have computed the absorbed γ -dose rate (D) of the Lonar samples (taking data from table 1 and literature) from the estimated abundances of ^{232}Th , ^{238}U , and ^{40}K using Eq. 1 (Fig. 5d). The palaeosol samples show the highest average D with relatively high standard deviation ($n = 9$, average \pm standard deviation: 18.34 ± 7.17 nGy h^{-1}), followed by the impact-melts and spherules ($n = 72$, 14.88 ± 2.55 nGy h^{-1} , and $n = 7$, 13.74 ± 1.45 nGy h^{-1} respectively), ejecta ($n = 19$, 8.42 ± 2.03 nGy h^{-1}) and target basalt ($n = 26$, 11.97 ± 3.37 nGy h^{-1}).

4 Discussion and Conclusions

The application of radioactivity is perhaps the least known technique in evaluating asteroid impact craters, probably due to its limitation observed in early studies (Rybach and Adams 1969). Our present field investigation on the radioactivity of Lonar samples, however, confirms that this method could be effectively used to map the geological distribution of the ejecta blanket around any deeply excavated terrestrial impact craters, if the target rocks are relatively old and have undergone a prolonged phase of weathering to produce in situ palaeosol. Our present investigation shows that the ejecta around the Lonar crater have ~ 1.3 and 1.9 times higher count rates of γ -rays in the field over the palaeosol and target basalt respectively (Table 2). So it can be concluded that radioactivity mapping (γ count rates) by direct measurement using a portable Geiger-Müller pulse counter in the field could be helpful for a better understanding of the ejecta distribution around any deeply excavated terrestrial impact craters on any relatively old target rocks/palaeosol rather any conventional mapping using field or satellite imagery techniques. The results could be more useful for bigger craters where the excavation due to asteroid impact can reach below the zones of weathering, bringing the fresh, relatively unaltered target rocks from depth as a major component of the ejecta. The above method could be more sensitive for the more radioactive granitoid targets, which have undergone prolonged phase of surface weathering.

The Lonar palaeosol, which has formed by insitu weathering of the Deccan basalts during last ~ 570 ka and presently underlying the ejecta around the rim of the Lonar crater, in principle should contain relatively low water soluble K and U compared to those in the ejecta. However, this palaeosol has a relatively high U content and equivalent amount of K in comparison to those in the ejecta (Fig. 5). When observed in cross section, the black-coloured palaeosol contains white calcified root casts that come out from the overlying light-brown ejecta (Maloof et al. 2010), indicating the activity of percolating surface water (importantly rain water) through the ejecta into the palaeosol. This downward migrating groundwater most likely removes the mobile K and U from the ejecta and concentrates these elements into the underlying palaeosol resulting in the present secondary geochemical distribution of water soluble radioactive elements, which is certainly a post-impact phenomenon.

The computed absorbed γ -doses rates (D) of the Lunar samples (Fig. 5d) are inconsistent with those observed in field measurement on γ -radiation (Fig. 4). While the ejecta have higher γ -count rates over the palaeosol in the field, we observe a reverse picture for the computed absorbed γ -dose rates (D). The most probable explanation could be that during our measurements using a Geiger–Müller counter in the field, we measured the total γ -radiation coming out of the surface including, most importantly, the emission from radiogenic radon. In the laboratory measurements, we only count the number of γ -rays in three distinct energy windows and do not at all consider the effect of radon during our computation. However, since the palaeosol and ejecta show distinctly different radiation levels both in the field and in computed D values, it can be concluded that measuring the γ -ray activity could be used as an effective tool for mapping the ejecta deposits both around the Lunar and other impact craters on the Earth and on other planetary bodies in our Solar system.

Acknowledgments We are indebted to the Director, National Geophysical Research Institute, Hyderabad, India, for helping us in analyses of our samples and to H. Newsom for his encouragement during the progress of this research. The guidance of A. Dube during our field work and various assistances from G. Parthasarathy are greatly acknowledged. We thank D. Sengupta, Indian Institute of Technology, Kharagpur, India, for various administrative assistances. We are grateful to T. Mukherjee for kindly permitting us to use her unpublished data, and to M. Gudipati and two anonymous reviewers for their constructive comments on the early version of the manuscript. Financial assistance for this work was provided by Planex, Indian Space Research Organization, India, and partly by the University of KwaZulu-Natal productivity research grant to one of us (S. M.).

Appendix

See Fig. 3.

Basic field data for Fig. 3a and c

Longitudes	Latitudes	γ (counts/min)
Basic field data for Fig. 3a*		
76.51328	19.9657	21
76.51215	19.9658	27
76.51113	19.9663	24
76.51383	19.9663	23
76.50883	19.9665	29
76.50895	19.9673	30
76.5088	19.9676	19
76.5113	19.9678	33
76.51438	19.9678	30
76.51002	19.9679	24
76.51917	19.9686	20
76.5189	19.9686	22
76.51863	19.9686	25
76.51836	19.9686	21
76.51809	19.9686	22
76.51782	19.9686	25
76.51755	19.9686	25
76.51728	19.9686	26

continued

Longitudes	Latitudes	γ (counts/min)
76.51701	19.9686	30
76.51674	19.9686	25
76.51647	19.9686	23
76.51633	19.9686	21
76.51606	19.9686	25
76.51579	19.9686	26
76.51552	19.9686	30
76.52931	19.9687	17
76.52648	19.9687	26
76.52305	19.9687	25
76.52332	19.9688	28
76.52228	19.9688	18
76.51997	19.9688	26
76.53043	19.9689	16
76.53016	19.9689	21
76.52958	19.9689	25
76.52145	19.9689	27
76.52931	19.9690	22
76.5252	19.9690	21
76.53043	19.9692	16
76.53016	19.9692	22
76.52931	19.9692	21
76.53043	19.9694	26
76.53016	19.9694	25
76.52989	19.9694	29
76.52962	19.9694	23
76.52796	19.9695	21
76.53043	19.9697	15
76.53016	19.9697	17
76.52989	19.9697	19
76.52962	19.9697	27
76.52796	19.9698	22
76.53043	19.9700	17
76.53016	19.9700	22
76.52989	19.9700	27
76.52962	19.9700	24
76.52796	19.9700	18
76.52796	19.9703	23
Basic field data for Fig. 3c*		
76.5113	19.96783	33
76.5088	19.96757	19
76.50895	19.96728	30
76.50883	19.96648	29
76.51113	19.96628	24

continued	Longitudes	Latitudes	γ (counts/min)
	76.51215	19.96578	27
	76.51328	19.96565	21
	76.51383	19.96628	23
* Associated error in each measurement is ± 1 count/min	76.5158	19.97037	14

References

- A.-L. Chenet, X. Quidelleur, F. Fluteau, V. Courtilot, S. Bajpai, ^{40}K - ^{40}Ar dating of the Main Deccan large igneous province: further evidence of KTB age and short duration. *Earth Planet. Sci. Lett.* **263**, 1–15 (2007)
- V. Courtilot, Y. Gallet, R. Rocchia, G. Féraud, E. Robin, C. Hofmann, N. Bhandari, Z.G. Ghevariya, Cosmic markers, $^{40}\text{Ar}/^{39}\text{Ar}$ dating and paleomagnetism of the KT sections in the Anjar area of the Deccan large igneous province. *Earth Planet. Sci. Lett.* **182**, 137–156 (2000)
- A.P. Crósta, C. Koeberl, R.A. Furuie, C. Kazzuo-Vieira, The first description and confirmation of the Vista Alegre impact structure in the Paraná flood basalts of southern Brazil. *Meteorit. Planet. Sci.* **45**, 181–194 (2010)
- G. Faure, *Principles of isotope geology*, 2nd edn. (Wiley, New York, 1986)
- V.I. Feldman, L.V. Sazonova, Y.V. Mironov, I.G. Kapustkina, Circular structure logancha as possible meteorite crater in basalts of the Tunguska syncline. 14th Lunar and Planetary Science Conference, pp. 191–192 (1983)
- K. Fredriksson, A. Dube, D.J. Milton, M.S. Balasundaram, Lonar Lake, India: an impact crater in basalt. *Science* **180**, 862–864 (1973)
- R.F. Fudali, D.J. Milton, K. Fredriksson, A. Dube, Morphology of Lonar crater, India: comparisons and implications. *Moon Planets* **23**, 493–515 (1980)
- S. Ghosh, S.K. Bhaduri, Petrography and petrochemistry of impact melts from Lonar crater, Buldhana district, Maharashtra, India. *Indian Miner.* **57**, 1–26 (2003)
- C. Hofmann, G. Féraud, V. Courtilot, $^{40}\text{Ar}/^{39}\text{Ar}$ dating of mineral separates and whole rocks from the Western Ghats lava pile: further constraints on duration and age of the Deccan traps. *Earth Planet. Sci. Lett.* **180**, 13–27 (2000)
- F. Jourdan, F. Moynier, C. Koeberl, S. Eroglu, $^{40}\text{Ar}/^{39}\text{Ar}$ age of the Lonar crater and consequence for the geochronology of planetary impacts. *Geology* **39**, 671–674 (2011)
- IMD (2013) Indian Meteorological Department, Government of India: Available online at <http://www.Imd.gov.in> (last accessed on 21 Jan 2013)
- C. Koeberl, N. Bhandari, D. Dhingra, P.O. Suresh, V.L. Narasimham, S. Misra, Lonar impact crater, India—occurrence of a basaltic suevite? 35th Lunar and planetary science conference, abstract no. 1751 (CD-ROM) (2004)
- P.S. Kumar, Structural effects of meteorite impact on basalt: evidence from Lonar crater, India. *J. Geophys. Res.* **110**, B12402 (2005)
- A.C. Maloof, S.T. Stewart, B.P. Weiss, S.A. Soule, N.L. Swanson-Hysell, K.L. Louzada, I. Garrick-Bethell, P.M. Poussart, Geology of Lonar crater, India. *Geol. Soc. Am. Bull.* **122**, 109–126 (2010)
- V.L. Masaitis, Impact structures of northeastern Eurasia: the territories of Russia and adjacent countries. *Meteorit. Planet. Sci.* **34**, 691–711 (1999)
- S. Master, Evidence for an impact origin of the Amber Lake structure: a smaller companion crater to Lonar impact crater, Maharashtra, India (abstract). *Meteorit. Planet. Sci.* **34**, A78 (1999)
- S. Misra, H.E. Newsom, Incompatible trace element fractionation in impact-melts of Lonar crater, India—evidence of differential impact melting of target Deccan basalt. 42nd Lunar and planetary science conference, abstract no. 1060 (CD-ROM) (2011)
- S. Misra, H.E. Newsom, M. Shyam Prasad, J.W. Geissman, A. Dube, D. Sengupta, Geochemical identification of impactor for Lonar crater, India. *Meteorit. Planet. Sci.* **44**, 1001–1018 (2009)
- S. Misra, Md Arif, N. Basavaiah, P.K. Srivastava, A. Dube, Structural and anisotropy of magnetic susceptibility (AMS) evidence for oblique impact on terrestrial basalt flows: Lonar crater, India. *Geol. Soc. Am. Bull.* **122**, 563–574 (2010)
- N.C. Nandy, V.B. Deo, Origin of the Lonar Lake and its alkalinity. *J. Tata Iron Steel Co.* **8**, 1–12 (1961)

- V.K. Nayak, Glassy objects (impactite glasses?) A possible new evidence for meteoritic origin of the Lonar crater, Maharashtra State, India. *Earth Planet. Sci. Lett.* **14**, 1–6 (1972)
- H.E. Newsom, S. Misra, M.J. Nelson, Aqueous alteration of the proximal and distal ejecta blanket at Lonar crater, India. 38th Lunar and planetary science conference, Abstract no. 2056 (CD-ROM) (2007)
- H.E. Newsom, S. Misra, S.P. Wright, N. Muttik, Contrasting alteration and enrichment of mobile elements during weathering of basaltic ejecta and ancient soil at Lonar crater, India. 41st Lunar and planetary science conference, abstract no. 2210 (CD-ROM) (2010)
- S. Osaе, S. Misra, C. Koeberl, D. Sengupta, S. Ghosh, Target rocks, impact-glasses, and melt rocks from the Lonar impact crater, India: petrography and geochemistry. *Meteorit. Planet. Sci.* **40**, 1473–1492 (2005)
- K. Pande, S.K. Pattanayak, K.V. Subbarao, P. Navaneethakrishnan, T.R. Venkatesan, ^{40}Ar - ^{39}Ar age of a lava flow from the Bhimashankar Formation, Giravali Ghat, Deccan Traps. *Proc. Indian Acad. Sci. (Earth Planet. Sci.)* **113**, 755–758 (2004)
- E. Pierazzo, H.J. Melosh, Understanding oblique impacts from experiments, observations, and modeling. *Annu. Rev. Earth Planet. Sci.* **28**, 141–167 (2000)
- U.R. Rao, Gamma-ray spectrometric set-up at NGRI for analysis of U, Th and K in rocks. *Geophys. Res. Bull.* **12**, 91–101 (1974)
- S.N. Rao, D. Sengupta, R. Guin, S.K. Saha, Natural radioactivity measurements in beach sand along southern coast of Orissa, eastern India. *Environ. Earth Sci.* **59**, 593–601 (2009)
- M.K. Reichow, A.D. Saunders, R.V. White, M.S. Pringle, A.I. Al'Mukhamedov, A.I. Medvedev, N.P. Kirda, $^{40}\text{Ar}/^{39}\text{Ar}$ dates from the West Siberian Basin: siberian flood basalt province doubled. *Science* **296**, 1846–1849 (2002)
- L. Rybach, J.A.S. Adams, The radioactivity of the Ivory Coast tektites and the formation of the Bosumtwi Crater (Ghana). *Geochim. Cosmochim. Acta* **33**, 1101–1102 (1969)
- D. Scherler, T. Kenkmann, A. Jahn, Structural record of an oblique impact. *Earth Planet. Sci. Lett.* **248**, 43–53 (2006)
- P.H. Schultz, C.A. Eberhardy, C.M. Ernst, M.F. A'Hearn, J.M. Sunshine, C.M. Lisse, The Deep impact oblique impact cratering experiment. *Icarus* **191**, 84–122 (2007)
- D. Sengupta, A. Ghosh, M.A. Mamtani, Radioactivity studies along fracture zones in areas around Galudih, east Singhbhum, Jharkhand, India. *Appl. Radiat. Isot.* **63**, 409–414 (2005)
- T.H. Son, C. Koeberl, Chemical variation in Lonar impact glasses and impactites. *GFF* **129**, 161–176 (2007)
- UNSCEAR, *Sources and effects of ionizing radiation* (United Nation Scientific Committee on the effect of Atomic Radiation, New York, 1993)
- UNSCEAR, *Sources and effects of ionizing radiation. Report to the general assembly with scientific annexes.* United Nations Scientific Committee on the effect of atomic radiation, New York (2000)
- W.M. White, *Geochemistry* (John-Hopkins University Press, USA, 2005). (on-line text book)